

Model-Based Detection of Heart Rate Turbulence

Kristian Solem*, Pablo Laguna, *Senior Member, IEEE*, Juan Pablo Martínez,
and Leif Sörnmo, *Senior Member, IEEE*

Abstract—In this study, the integral pulse frequency modulation model is extended to account for the presence of ectopic beats and heart rate turbulence (HRT). Based on this model, a new statistical approach to the detection and characterization of HRT is presented. The detector structure involves a set of Karhunen–Loève basis functions and a generalized likelihood ratio test statistic $T(x)$. The three most significant basis functions reflect the difference in heart rate prior to a ventricular ectopic beat (VEB) compared to after HRT, the “average” HRT, and a delayed contribution to HRT, respectively. Detector performance was studied on both simulated and ECG signals. Three different simulations were performed for the purpose of studying the influence of SNR, QRS jitter, and ECG sampling rate. The results show that the HRT test statistic $T(x)$ performs better in all simulations than do the commonly used parameters known as turbulence onset (TO) and turbulence slope (TS). In order to attain the same performance as $T(x)$, TS needs at least twice the amount of VEBs for averaging, and TO at least four times. The detector performance was also studied on ECGs acquired from eight patients who underwent hemodialysis treatment with the goal to discriminate between patients considered to be hypotension-resistant (HtR) and hypotension-prone (HtP). The results show that $T(x)$ exhibits larger mean values in HtR patients than in HtP, suggesting that HRT is mostly present in HtR patients. The overlap between the two groups was larger for TO and TS than for $T(x)$.

Index Terms—ECG, generalized likelihood ratio test (GLRT), heart rate turbulence (HRT), integral pulse frequency modulation (IPFM) model, Karhunen–Loève (KL) basis functions.

I. INTRODUCTION

THE SHORT-TERM fluctuation in heart rate that follows a ventricular ectopic beat (VEB) is referred to as heart rate turbulence (HRT) [1], [2]. In normal subjects, the heart rate first increases and then decreases to baseline, immediately after a VEB. The increase in heart rate is hypothesized to be due to compensation of the sudden drop in blood pressure induced by the VEB, and subsequently, sensed by the baroreceptors [3]–[7]. Once blood pressure is restored, the heart rate returns to baseline

Manuscript received October 22, 2007; revised March 10, 2008. First published November 17, 2008; current version published December 17, 2008. This work was supported by grants from Gambro AB, Lund, Sweden, The Swedish Research Council, Comisión Interministerial de Ciencia y Tecnología (CICYT) (TEC2007-68076-C02-02), and the Grupo Consolidado T30, DGA, Spain. *Asterisk indicates corresponding author.*

*K. Solem is with the Signal Processing Group, Department of Electrical and Information Technology, Lund University, S-221 00 Lund, Sweden (e-mail: kristian.solem@eit.lth.se).

P. Laguna and J. P. Martínez are with the Communications Technology Group, Aragón Institute for Engineering Research, University of Zaragoza, E-50018 Zaragoza, Spain, and also with the Investigación Biomédica en Red en Bioingeniería, Biomateriales y Nanomedicina (CIBER-BBN), E-50018 Zaragoza, Spain.

L. Sörnmo is with the Signal Processing Group, Department of Electrical and Information Technology, Lund University, S-221 00 Lund, Sweden.

Color versions of one or more of the figures in this paper are available online at <http://ieeexplore.ieee.org>.

Digital Object Identifier 10.1109/TBME.2008.2002113

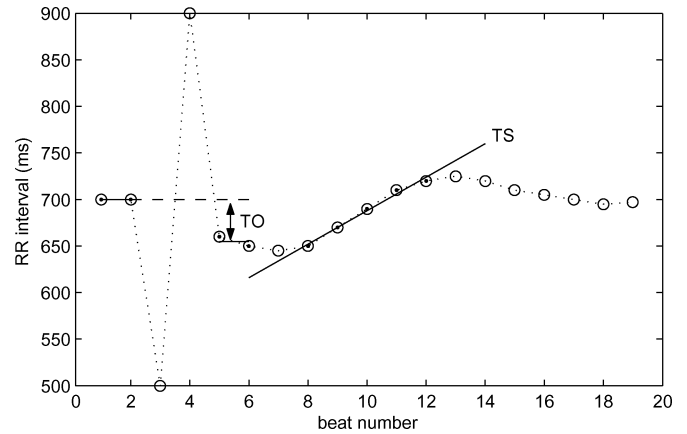


Fig. 1. HRT in the RR interval tachogram for a normal subject. Beat numbers 3 and 4 are the shortened and prolonged RR intervals induced by a VEB (the coupling interval and the compensatory pause). The parameters TO and TS are also illustrated.

in order to maintain the blood pressure. The subject’s ability to recover from a local decrease in blood pressure is reflected by the strength of turbulence. The absence of HRT reflects autonomic dysfunction [3], [4].

It has been demonstrated that HRT is a powerful predictor of mortality after acute myocardial infarction [1], [2]. The analysis of HRT offers considerable potential in other areas as well, e.g., congestive heart failure, diabetes mellitus [3], [4], and hypotension in hemodialysis patients [8]. Several parameters for HRT characterization have been presented of which turbulence onset (TO) and turbulence slope (TS) are the most commonly employed (see Fig. 1). The parameter TO is the relative difference of RR intervals enclosing a VEB, defined by the relative difference of the averages of the two normal RR intervals before and after the VEB. Since TO measures the relative change in RR intervals, negative values of TO imply heart rate acceleration following the VEB, whereas positive values imply heart rate deceleration. The parameter TS is defined by the steepest slope observed over five consecutive RR intervals in the first 15 RR intervals following the VEB (see Fig. 1). Prior to computation of TO and TS, an average RR interval tachogram is determined from available VEBs.

While both TO and TS have proven to be clinically useful, they are empirical in nature as they do not result from data modeling. Several studies have shown that TS is clinically more powerful than TO, e.g., as a predictor of mortality after acute myocardial infarction [1]–[4]. However, TS has certain drawbacks. First, TS is overestimated at low SNRs, i.e., when few VEBs are used for averaging or when the underlying heart rate variability (HRV) is considerable [9]. Second, TS leads to structural correlation between HRT and heart rate [9].

Besides TO and TS, several other HRT parameters have been presented of which the majority are closely related to TO and TS, such as combined TO and TS analysis [4], and an adjusted TS parameter with respect to either heart rate or the number of averaged beats [9]. Furthermore, the first beat number of the 5 RR interval sequence from which TS is determined (i.e., where the steepest slope of RR intervals is observed) is denoted turbulence timing [10]. The correlation coefficient of TS is defined as the correlation coefficient of the regression line fitted to the 5 RR intervals of TS [11]. Other parameters are the turbulence jump, defined as the maximum difference between adjacent RR intervals [12], and the turbulence dynamics, quantifying the correlation between TS and heart rate [13]. Yet another measure is the turbulence frequency decrease that results from fitting a sine function to the RR intervals following the compensatory pause [4].

The purpose of the present paper is to develop a model-based technique for HRT characterization, and to compare its performance to that of TO and TS, using both simulated and clinical data. Based on an extended integral pulse frequency modulation (IPFM) model, we present an approach that involves a set of Karhunen–Loève (KL) basis functions, modeling HRT as a uniformly sampled function of time. This stands in contrast to existing HRT parameters that are computed from the RR interval series. The interval series is a function of beat index and is thus an irregularly sampled function of time. The KL representation is then used in a statistical HRT detection procedure. The clinical issue of the present study is to investigate whether HRT can be used to distinguish between hemodialysis patients considered to be hypotension-resistant (HtR) and hypotension-prone (HtP) patients.

II. METHODS

A. Extended IPFM Model

The original IPFM model was introduced to generate a series of occurrence times for sinus beats with known rate variability, reflecting basic electrophysiological properties of the sinoatrial node [14], [15]. The model input signal is the sum of a dc level, accounting for mean heart rate, and a zero-mean modulating signal $m(t)$, accounting for variability due to both parasympathetic and sympathetic activity [see Fig. 2(a)].

The input signal is integrated until a threshold T_0 is reached, representing the mean interval length between successive events. An event is created at time t_k as the output of the model, and the integrator is reset to zero. As a result, the output signal of the IPFM model becomes an event series that represents the beat occurrence times. In mathematical terms, the following equation defines the series of event times:

$$\int_0^{t_k} (1 + m(\tau)) d\tau = kT_0, \quad k = 0, \dots, K \quad (1)$$

where k is an integer that indexes the k th beat following the initial event assumed to occur at $t_0 = 0$.

The heart timing signal $d_{HT}(t)$ is at time t_k defined as the difference between the expected occurrence time at the mean

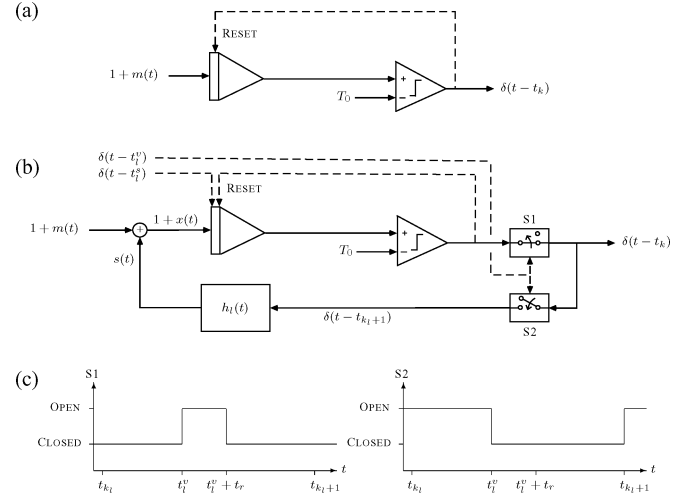


Fig. 2. (a) Block diagram of the original IPFM model. (b) Block diagram of the extended IPFM model. (c) Switches, S1 and S2, in the extended IPFM model. The switches in (b) are drawn in the state of a normal sinus rhythm. Dashed lines describe control signals.

heart rate kT_0 and t_k [16]. It has been shown that the heart timing signal is closely related to the IPFM model and its modulating signal $m(t)$ [15]. In order to clarify this relation, the model equation in (1) is rewritten for a particular t_k so that

$$\int_0^{t_k} m(\tau) d\tau = kT_0 - t_k \equiv d_{HT}(t_k) \quad (2)$$

where T_0 must be estimated from the available data before $d_{HT}(t_k)$ can be computed. Thus, $m(t)$ is the derivative of $d_{HT}(t)$, the former reflecting the membrane potentials of the sinoatrial cells.

During sinus rhythm, the electrophysiological influence of a supraventricular ectopic beat (SVEB) may be viewed as a reset of the charging potentials in the sinoatrial node. In order to incorporate this property in the IPFM model, the integrator has to be reset at t_l^s corresponding to the l th SVEB [see Fig. 2(b)].

A normal heartbeat will induce an electrical wave propagating from the atria to the ventricles, whereas a VEB will induce a retrograde wave propagating from the ventricles to the atria [17]. The electrical wave from a normal heartbeat will not arrive to the ventricles if a VEB is present, since the wave will be interrupted by the retrograde wave induced by the VEB. In the extended model, proposed in this paper, this interruption is accounted for by the switch S1 that opens at t_l^s , corresponding to the occurrence time of the l th VEB, and which closes at $t_l^s + t_r$, where t_r corresponds to the ventricular refractory period [see Fig. 2(b) and (c)]. These modifications account for SVEBs and VEBs when generating the occurrence times of normal sinus beats without turbulence.

In order to account for the HRT phenomenon, additional feedback is introduced in the model. Physiologically, HRT is triggered at t_{k+1} by the diastolic blood pressure drop induced by the VEB, where t_{k+1} denotes the occurrence time of the first normal sinus beat that follows the l th VEB. The first normal

sinus beat before the l th VEB is denoted as t_{k_l} , so the sequence of beat times is

$$\dots, t_{k_l}, t_l^v, t_{k_l+1}, \dots$$

HRT is incorporated by feedback involving a linear system with impulse response $h_l(t)$, where $h_l(t)$ is the turbulence associated with the l th VEB [see Fig. 2(b)]. The feedback branch models the baroreceptors so that HRT is triggered by an impulse fed to the linear system at t_{k_l+1} . The summation of all different HRTs, denoted $s(t)$, caused by different VEBs, i.e.,

$$s(t) = \sum_{l=1}^{N_e} h_l(t - t_{k_l+1}) \quad (3)$$

is added to the input of the integrator of the IPFM model; N_e denotes the number of VEBs. Consequently, $d_{HT}(t_k)$ in (2) is redefined according to

$$\begin{aligned} \int_0^{t_k} x(\tau) d\tau &= \int_0^{t_k} (m(\tau) + s(\tau)) d\tau = kT_0 - t_k \\ &\equiv d_{HT}(t_k). \end{aligned} \quad (4)$$

The impulse response $h_l(t)$ is causal and returns to zero when the turbulence has vanished. It is assumed that $h_{l-1}(t - t_{k_{l-1}+1})$ returns to zero prior to the onset of the subsequent HRT $h_l(t - t_{k_l+1})$ since in practice, HRT is only analyzed when the distance between successive VEBs is sufficiently large, i.e., at least 15 beats [2].

In this paper, HRT is modeled as a linear combination of basis functions,

$$h_l(t) = \mathbf{b}^T(t) \boldsymbol{\theta}_l \quad (5)$$

where $\mathbf{b}(t) = [b_1(t) \ b_2(t) \ \dots \ b_r(t)]^T$ contains r basis functions and $\boldsymbol{\theta}_l$ is an $r \times 1$ weight vector associated with the l th VEB. Thus, the extended IPFM model accounts for variations in both HRT dynamics and amplitude through $\mathbf{b}(t)$ and $\boldsymbol{\theta}_l$. The dynamics of HRT is characterized by $\mathbf{b}(t)$ and determined from a learning dataset, whereas the weights $\boldsymbol{\theta}_l$ define the turbulence shape in the l th VEB.

B. KL Basis Functions

In this study, data-dependent basis functions are considered, and in particular, the KL basis functions since these are optimal for a given set of data. The KL basis functions are obtained as the most significant eigenvectors of the mean correlation matrix $\bar{\mathbf{R}}_x$ that results from subjects with HRT. For each subject, the sample correlation matrix \mathbf{R}_x is obtained by

$$\mathbf{R}_x = \frac{1}{N_e} \sum_{l=1}^{N_e} \mathbf{x}_l \mathbf{x}_l^T \quad (6)$$

where \mathbf{x}_l is an $N \times 1$ vector with HRT data from the l th VEB in a subject. In order to obtain \mathbf{x}_l , an estimate of the input $x(t)$ to the IPFM model is derived from a second-order approximation to the derivative of $d_{HT}(t)$ [cf. (4)] according to

$$\begin{aligned} \frac{d}{dt} d_{HT}(t_k) &= x(t_k) \approx \frac{2T_0}{t_{k+1} - t_{k-1}} - 1 \\ k &= k_l + 2, k_l + 3, \dots, \quad l = 1, 2, \dots, N_e. \end{aligned} \quad (7)$$

For each subject, the mean RR interval T_0 in (7) is estimated from the 10 RR intervals that precede each VEB,

$$T_0 = \frac{1}{N_e} \sum_{l=1}^{N_e} \frac{t_{k_l} - t_{k_l-10}}{10} \quad (8)$$

where t_{k_l} is the occurrence time of the sinus beat immediately prior to the l th VEB.

For the l th VEB, the input signal $x_l(t)$ to the IPFM model is obtained from $x(t)$ according to

$$x_l(t_k) = \begin{cases} 0, & k = 0, \dots, k_l + 1 \\ x(t_k), & k = k_l + 2, \dots \end{cases}, \quad l = 1, 2, \dots, N_e. \quad (9)$$

The definition in (9) implies that t_{k_l+1} is the trigger time of the l th HRT, and that (7) can be applied. Since t_k is unevenly spaced, further processing is required to produce the evenly sampled vector \mathbf{x}_l . This vector results from interpolation of $x_l(t_k)$ to produce $x_l(t)$ and followed by equidistant resampling of $x_l(t)$. Using a sampling rate of F_s Hz, resampling starts at t_{k_l+1} to assure that \mathbf{x}_l contains the HRT from its very onset,

$$\mathbf{x}_l = \begin{bmatrix} x_l(t_{k_l+1}) \\ x_l\left(t_{k_l+1} + \frac{1}{F_s}\right) \\ \vdots \\ x_l\left(t_{k_l+1} + \frac{N-1}{F_s}\right) \end{bmatrix}. \quad (10)$$

Note that HRT is assumed to start after t_{k_l+1} , cf. (9). If it would start before t_{k_l+1} , it could not be reflected in the RR series in any case. It should be noted that the first normal RR interval after the VEB is between t_{k_l+1} and t_{k_l+2} .

Once \mathbf{R}_x is estimated for each of the subjects, the mean correlation matrix $\bar{\mathbf{R}}_x$ for all subjects is determined. The r most significant eigenvectors of $\bar{\mathbf{R}}_x$ are chosen as the discrete representation of the basis functions contained in $\mathbf{b}(t)$. Thus, (5) becomes

$$\mathbf{h}_l = \mathbf{B} \boldsymbol{\theta}_l \quad (11)$$

where \mathbf{h}_l is an $N \times 1$ vector with the discrete representation of the HRT associated with the l th VEB, and \mathbf{B} is an $N \times r$ matrix with the r most significant eigenvectors in its columns,

$$\mathbf{B} = \begin{bmatrix} \mathbf{b}^T(0) \\ \mathbf{b}^T\left(\frac{1}{F_s}\right) \\ \vdots \\ \mathbf{b}^T\left(\frac{N-1}{F_s}\right) \end{bmatrix}. \quad (12)$$

C. HRT Detection

Our approach to detect and characterize HRT is based on the extended IPFM model, and in particular, the linear model in (11). The detection procedure is formulated as one in which

HRT is either absent (hypothesis \mathcal{H}_0) or present (hypothesis \mathcal{H}_1),

$$\begin{aligned}\mathcal{H}_0 &: \mathbf{x} = \mathbf{m} \\ \mathcal{H}_1 &: \mathbf{x} = \mathbf{B}\boldsymbol{\theta} + \mathbf{m}.\end{aligned}\quad (13)$$

Here, \mathbf{x} is an $N \times 1$ vector with the observed data, \mathbf{m} is an $N \times 1$ vector considered as random white noise characterized by a Gaussian probability density function (pdf) $\mathcal{N}(\mathbf{0}, \sigma^2 \mathbf{I})$ with σ^2 as unknown parameter, \mathbf{B} is a known $N \times r$ ($r \leq N$) orthogonal matrix, and $\boldsymbol{\theta}$ is an $r \times 1$ vector with unknown weights. The noise term \mathbf{m} signifies undesired signal components, accounting for errors introduced by sampling of the ECG and QRS detection. The noise term may also account for the presence of HRV when some components of HRV remain in play during turbulence. The detector design is here based on a “least informative” approach where no assumption is made on noise color (also see Section V).

The design of the HRT detector is based on the Neyman–Pearson theorem [18], which maximizes the probability of detection P_D for a given probability of false alarm $P_{FA} = \alpha$ by deciding \mathcal{H}_1 if

$$L(\mathbf{x}) = \frac{p(\mathbf{x}; \mathcal{H}_1)}{p(\mathbf{x}; \mathcal{H}_0)} > \gamma \quad (14)$$

where $p(\mathbf{x}; \mathcal{H}_i)$ denotes the pdf of \mathbf{x} under \mathcal{H}_i , and the threshold γ is found from

$$P_{FA} = \int_{\{\mathbf{x}: L(\mathbf{x}) > \gamma\}} p(\mathbf{x}; \mathcal{H}_0) d\mathbf{x} = \alpha. \quad (15)$$

However, the pdfs in (13) contain unknown parameters, i.e., σ^2 and $\boldsymbol{\theta}$. Employing the generalized likelihood ratio test (GLRT), the unknown parameters are first estimated with maximum likelihood estimation (MLE), and then, inserted into the likelihood ratio test $L(\mathbf{x})$ [18]. With the hypothesis test in (13), the GLRT decides \mathcal{H}_1 if

$$L_G(\mathbf{x}) = \frac{p(\mathbf{x}; \hat{\boldsymbol{\theta}}, \hat{\sigma}_{\mathcal{H}_1}^2, \mathcal{H}_1)}{p(\mathbf{x}; \hat{\sigma}_{\mathcal{H}_0}^2, \mathcal{H}_0)} > \gamma \quad (16)$$

where $\hat{\boldsymbol{\theta}}$ and $\hat{\sigma}_{\mathcal{H}_1}^2$ are the MLEs of $\boldsymbol{\theta}$ and σ^2 , respectively, assuming that \mathcal{H}_1 is true (jointly maximize $p(\mathbf{x}; \boldsymbol{\theta}, \sigma^2, \mathcal{H}_1)$), and $\hat{\sigma}_{\mathcal{H}_0}^2$ is the MLE of σ^2 assuming that \mathcal{H}_0 is true [maximizes $p(\mathbf{x}; \sigma^2, \mathcal{H}_0)$].

The resulting test statistic $T(\mathbf{x})$ of the GLRT in (16) is used for HRT detection (see the Appendix). Hypothesis \mathcal{H}_1 is decided if

$$T(\mathbf{x}) = \frac{N-r}{r} \frac{\hat{\boldsymbol{\theta}}^T \hat{\boldsymbol{\theta}}}{\mathbf{x}^T \mathbf{x} - \hat{\boldsymbol{\theta}}^T \hat{\boldsymbol{\theta}}} = \frac{N-r}{r} \frac{\mathbf{x}^T \mathbf{B} \mathbf{B}^T \mathbf{x}}{\mathbf{x}^T (\mathbf{I} - \mathbf{B} \mathbf{B}^T) \mathbf{x}} > \gamma' \quad (17)$$

where $\hat{\boldsymbol{\theta}} = \mathbf{B}^T \mathbf{x}$ and γ' is a threshold determined by a given P_{FA} . The energy projected on the signal space (spanned by r basis functions) is given by $\mathbf{x}^T \mathbf{B} \mathbf{B}^T \mathbf{x}$, whereas the energy projected on the orthogonal $(N-r)$ -dimensional noise space is given by $\mathbf{x}^T (\mathbf{I} - \mathbf{B} \mathbf{B}^T) \mathbf{x}$. As a result, the test statistic $T(\mathbf{x})$ can be viewed as an estimate of the SNR that reflects the ratio between HRT and HRV.

D. HRT Averaging

In contrast to existing HRT studies, this study does not assume that HRT is based on averaged data, i.e., $\boldsymbol{\theta}_l$ can be estimated from a single VEB. In case averaging is combined with the GLRT detector, the observations in (17) are replaced with

$$\mathbf{x} = \frac{1}{N_e} \sum_{l=1}^{N_e} \mathbf{x}_l. \quad (18)$$

Due to the linear HRT model, $\boldsymbol{\theta}$ will represent the weights for the averaged HRT and are obtained in a way analogous to (18), i.e.,

$$\boldsymbol{\theta} = \frac{1}{N_e} \sum_{l=1}^{N_e} \boldsymbol{\theta}_l. \quad (19)$$

E. HRT Time Scaling

Coupling between HRT duration and heart rate is implicit to both TO and TS as they depend on beat index, whereas it is not for the present HRT detector. If such coupling would be present, it is natural to assume that increased heart rate is associated with shorter HRT duration and *vice versa*. In terms of the IPFM model, such coupling can be incorporated by normalizing the input signals $x_l(t)$ in (9) with respect to mean heart rate,

$$x_l \left(\frac{\bar{T}_0}{T_0} t_k \right) = \begin{cases} 0, & k = 0, \dots, k_l + 1 \\ x(t_k), & k = k_l + 2, \dots \end{cases}, \quad l = 1, 2, \dots, N_e \quad (20)$$

where the time axis is scaled with \bar{T}_0/T_0 ; \bar{T}_0 denotes the overall mean RR interval for all VEBs in all subjects.

The vector \mathbf{x}_l is then obtained from interpolation of (20) followed by resampling of $x_l(t)$, starting at $(\bar{T}_0/T_0)t_{k_l+1}$ in order to assure that \mathbf{x}_l contains the HRT from its very onset. The sample correlation matrix \mathbf{R}_x is determined by (6), after which the mean correlation matrix $\bar{\mathbf{R}}_x$ is determined. Finally, the r most significant eigenvectors of $\bar{\mathbf{R}}_x$ are chosen as the discrete representation of $\mathbf{b}(t)$.

III. DATA AND PERFORMANCE MEASURES

A. Simulation

The extended IPFM model is used to evaluate the performance of HRT detection. In this model, the mean interval length is set to $T_0 = 0.8$ s, i.e., a heart rate of 75 bpm, as this is the mean heart rate in the European ST-T database (see later). The shape of $h_l(t)$ is fixed and deterministic, obtained from the KL representation of the averaged HRT from the learning set described later. The underlying HRV, being modeled by $m(n)$ as the discrete representation of $m(t)$, is obtained as the output of a seventh-order autoregressive (AR) model with white noise as input [see Fig. 3(a)]. The power spectrum $S_m(e^{j\omega})$ of $m(n)$ is given by

$$S_m(e^{j\omega}) = \sigma_w^2 |H(e^{j\omega})|^2 = \frac{\sigma_w^2}{|1 + \sum_{q=1}^7 a_q e^{-j\omega q}|^2} \quad (21)$$

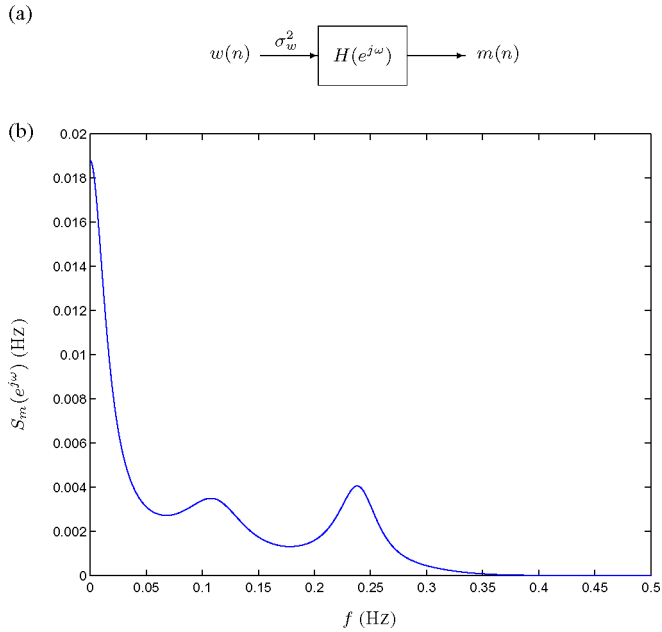


Fig. 3. (a) HRV is modeled as the output $m(n)$ of a linear system $H(e^{j\omega})$ fed by white noise $w(n)$. (b) Power spectrum of $m(n)$.

where

$$(a_1, \dots, a_7) = (-1.6265, 1.8849, -1.8327, 1.2970, \\ -0.7758, 0.4133, -0.2136)$$

and $\sigma_w^2 = 0.000404$ [16], using a sampling rate of 1 Hz of $m(t)$. Note that this sampling rate influences $m(t)$, but is unrelated to the mean heart rate used in the simulation model that can have any value higher than 60 bpm [i.e., “physiological” sampling of $m(t)$ at a rate higher than 1 Hz] as long as the HRV spectrum is confined to 0–0.5 Hz. If the spectral content of $m(t)$ exceeds 0.5 Hz, the heart rate should be at least twice the maximum spectral component of $m(t)$ in order to avoid aliasing [19]. The power spectrum $S_m(e^{j\omega})$ is displayed in Fig. 3(b).

Three types of simulations were performed in order to evaluate HRT detector performance. The first type evaluated performance at different SNRs. The SNR associated with the l th VEB was calculated according to

$$\text{SNR}_l = 10 \log_{10} \left(\frac{\mathbf{h}_l^T \mathbf{h}_l}{\mathbf{m}_l^T \mathbf{m}_l} \right) \quad (22)$$

where \mathbf{m}_l is an $N \times 1$ vector with the samples of $m(n)$ associated with the l th VEB. Different SNRs were obtained by changing the relation between the energy in \mathbf{h}_l and \mathbf{m}_l (weighting \mathbf{h}_l with a suitable factor) before adding them to the input of the extended model. Thus, the noise power was fixed, whereas the signal energy was changed to produce different SNRs.

The second type of simulation evaluated the influence of QRS detection inaccuracies on HRT detection. Such inaccuracies were studied by adding zero-mean Gaussian noise to the occurrence times of the sinus beats t_k produced by the extended model.

The third type of simulation evaluated the influence of different sampling rates F_r of the original ECG signal on HRT detection. This was studied by adding zero-mean uniform noise, $[-1/2F_r, 1/2F_r]$, to the occurrence times t_k to account for time quantization errors.

The performance was measured by the probability of detection P_D and the probability of false alarm P_{FA} , obtained by

$$P_D = \frac{N(\mathcal{H}_1|\mathcal{H}_1)}{N(\mathcal{H}_1|\mathcal{H}_1) + N(\mathcal{H}_0|\mathcal{H}_1)} \quad (23)$$

and

$$P_{FA} = \frac{N(\mathcal{H}_1|\mathcal{H}_0)}{N(\mathcal{H}_1|\mathcal{H}_0) + N(\mathcal{H}_0|\mathcal{H}_0)} \quad (24)$$

respectively, where $N(\mathcal{H}_i|\mathcal{H}_j)$ denotes the number of \mathcal{H}_i decisions when \mathcal{H}_j is true. Thus, $N(\mathcal{H}_1|\mathcal{H}_1)$ denotes when HRT is present and detected, $N(\mathcal{H}_0|\mathcal{H}_1)$ when HRT is present but missed (missed turbulence), $N(\mathcal{H}_1|\mathcal{H}_0)$ when HRT is absent but detected (false alarm), and $N(\mathcal{H}_0|\mathcal{H}_0)$ when HRT is correctly decided as absent.

Different values of P_{FA} were obtained by changing the detection threshold γ' for the HRT parameter of interest. Detection performance is presented using the receiver operating characteristic (ROC) in which P_D is displayed versus P_{FA} . It should be noted that the definitions of P_D and P_{FA} are the same for TO and TS as for $T(\mathbf{x})$. The difference to the standard evaluation of TO and TS is that we are not using fixed threshold values (i.e., TO = 0%, TS = 2.5 ms/beat), but allow them to change. For different threshold values, P_D and P_{FA} are determined for the parameters TO, TS, and $T(\mathbf{x})$.

B. ECG Datasets

The basis functions were determined from the European ST-T database that contains ambulatory two-lead ECG recordings (sampled at a rate of 250 Hz) from patients with myocardial ischemia, see [20] for further information on the database, and, e.g., [21] and [22] for its use in HRV analysis. Annotation information on beat occurrence times and beat categories, including VEB, is included in the database. In the present study, a total of 31 patients were selected from the database since they all fulfilled the requirement of having VEBs separated by at least 15 sinus beats. The selection resulted in 84 VEBs that were used as learning set. The signal vector \mathbf{x}_l resulted from resampling of $x_l(t)$ during a time interval of 10 s using $F_s = 2$ Hz, i.e., $N = 21$. The three most significant KL basis functions were chosen as the columns in \mathbf{B} , i.e., $r = 3$.

The HRT test statistic $T(\mathbf{x})$ was, together with TO and TS, studied on a target dataset that consisted of patients with end-stage renal failure who underwent regular hemodialysis treatment three times a week. The goal was to distinguish between patients considered HtR and HtP. Four patients were included in each group from a total of 16 patients once patients with VEBs separated by less than 15 sinus beats or with atrial fibrillation during the course of the recording had been excluded. Evidently, patients without VEBs were also excluded. Before the ECG was recorded, a physician classified each patient into one of the two groups based on the patient’s clinical history, such as the number

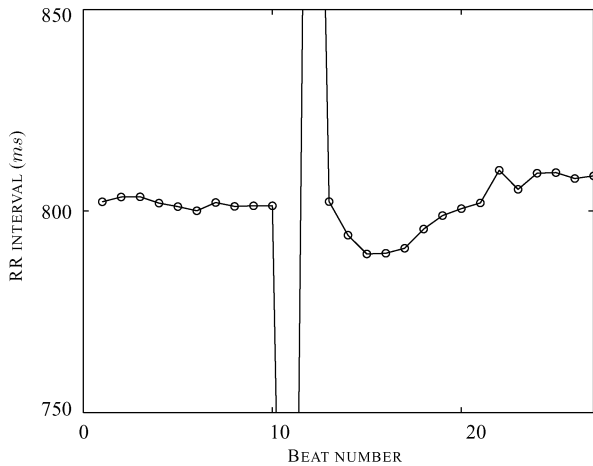


Fig. 4. Averaged RR interval tachogram from 84 VEBs in 31 myocardial ischemic patients, with $TO = -0.4\%$ and $TS = 3.2$ ms/beat. Beat numbers 11 and 12 are the coupling interval and the compensatory pause, respectively.

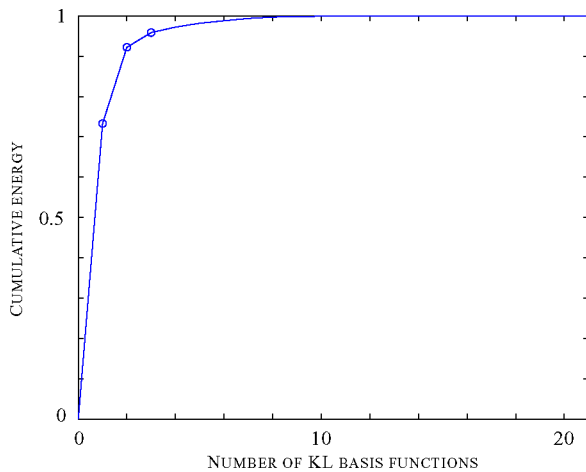


Fig. 5. Cumulative energy as reflected by the number of KL basis functions. The cumulative energy was obtained as the cumulative sum of eigenvalues, divided by the sum of all eigenvalues.

of hypotension episodes per month. The ECGs were acquired during clinical treatment at Park Dialys (Lund, Sweden) and Helsingborg Hospital (Sweden), lasting from 3 to 5 h. The ECG sampling rate was $F_r = 1000$ Hz. The study was approved by the local ethics committee.

IV. RESULTS

A. Basis Functions

The European ST-T database with ischemic patients was assessed with respect to HRT, and the averaged RR interval tachogram from the 84 VEBs was determined (see Fig. 4). The parameters TO and TS were determined, resulting in -0.4% and 3.2 ms/beat, respectively ($TO < 0\%$ and $TS > 2.5$ ms/beat are considered normal). Thus, HRT is present in the database, although not guaranteed in all the patients (see Section V).

The three most significant KL basis functions, obtained according to Section II-B, accounted together for 96% of the total energy from the total of 21 KL basis functions (see Fig. 5).

These three functions may be given the following interpretation: the most significant basis function have the shape of a step function, the second reflects the “average” HRT, and the third reflects a delayed contribution to HRT (see Fig. 6). It is common that the heart rate prior to a VEB and after the HRT differs. This offset in heart rate is reflected by the first basis function, e.g., a positive weight indicate a higher heart rate after the HRT than prior to the VEB. The significance of the first basis function is obscured when the averaged HRT is obtained from several VEBs, since the offset tends to be canceled by averaging. This can be observed in the averaged HRT, which is almost entirely described by the second basis function, while the contribution from the first and the third are negligible (see Figs. 4 and 6).

B. Simulation

The detection performances of $T(\mathbf{x})$ and TS are similar and virtually error free at 10 dB SNR, while the performance of TO is inferior (see Fig. 7). It is obvious from this diagram that the performance of $T(\mathbf{x})$ is superior to that of TO and TS when the SNR decreases.

Different SNRs may be interpreted as different numbers of VEBs used for averaging. The detection parameter P_D is displayed as a function of the SNR for a fixed $P_{FA} = 0.05$ in order to relate the performance of the different HRT detectors to averaging (see Fig. 8). The horizontal differences between the curves in Fig. 8 can be interpreted as a power gain of $T(\mathbf{x})$ with respect to TO and TS . For $P_D = 0.95$, there is a 6 dB gain between $T(\mathbf{x})$ and TO , and a 3 dB gain between $T(\mathbf{x})$ and TS . This means that $T(\mathbf{x})$ achieves the same performance as TO , using only one-fourth of the number of VEBs for averaging, and the same performance as TS with only half the number of VEBs, assuming that HRT and noise in different VEBs are uncorrelated [15]. In addition, TS achieves the same performance as TO with only half the number of VEBs for averaging, since there is a 3 dB power gain between them.

The influence of QRS detection inaccuracies on HRT detection was studied for $T(\mathbf{x})$, TO , and TS (see Fig. 9). The detection performance of $T(\mathbf{x})$ is unaffected by QRS jitter with a standard deviation of 0.5 ms, whereas TO and TS are slightly reduced (see Fig. 9). If the standard deviation is larger than 0.5 ms, the performance of $T(\mathbf{x})$ is superior to both TO and TS (see Fig. 9).

The influence of the sampling rate F_r of the original ECG signal on HRT detection was found to be negligible for all detectors when $F_r = 1000$ Hz was used (see Fig. 10). However, for lower rates, the performance of $T(\mathbf{x})$ was vastly superior to both TO and TS . For example, with a sampling rate of $F_r = 250$ Hz and a $P_{FA} = 0.05$, P_D for $T(\mathbf{x})$, TS , and TO were 100%, 64%, and 38%, respectively (see Fig. 10).

C. Real Data

The parameters $T(\mathbf{x})$, TO , and TS were calculated for the eight hemodialysis patients. The averaged HRT from each patient was used in the calculation of the different HRT parameters. In the calculation of $T(\mathbf{x})$, the averaged HRT was obtained by (18), and in the calculation of TO and TS , the averaged tachogram was used. The results of all three HRT parameters

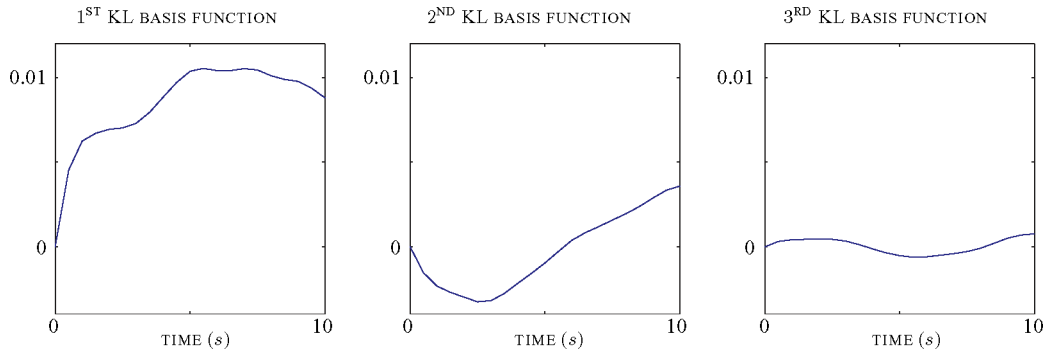


Fig. 6. Three most significant KL basis functions, weighted with their respective eigenvalues. The first KL basis functions is the most significant, and so forth.

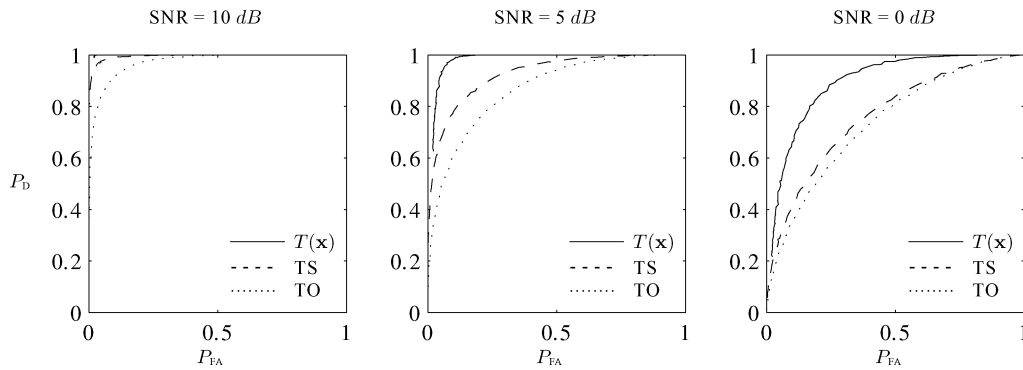


Fig. 7. ROC curves for different SNRs.

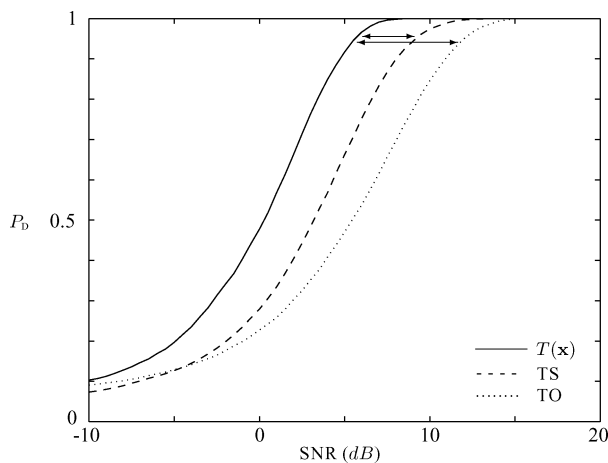


Fig. 8. P_D as a function of the SNR, for $P_{FA} = 0.05$. The power gain is 6 dB between $T(\mathbf{x})$ and TO, and 3 dB between $T(\mathbf{x})$ and TS, for $P_D = 0.95$.

suggest that HRT is more present in HtR than in HtP patients, when comparing the mean values of the two groups (see Table I). There was a larger overlap in TS between the patients in the two groups, when compared to $T(\mathbf{x})$, and a much larger overlap in TO when compared to both TS and $T(\mathbf{x})$ (see Table I). Thus, $T(\mathbf{x})$ appears to be better suited to distinguish between HtR and HtP patients, since the separation of the patients in the two groups is better than for TS, and much better than for TO.

D. HRT Time Scaling

The three most significant KL basis functions accounted together for 95% of the total energy from the 21 obtained KL basis functions, which is slightly lower than without scaling (i.e., 96%). These three basis functions are similar to those obtained without scaling and displayed in Fig. 6. The detection performance would improve if the heart rate influenced the duration of HRT with respect to time. However, the separation between HtR and HtP hemodialysis patients did not improve when scaling was included.

The results suggest that the heart rate does not influence HRT duration with respect to time, since the performance did not improve, but rather deteriorated with scaling.

V. DISCUSSION

This paper introduces a model-based approach to HRT detection and demonstrates on simulated data that the achieved performance is superior to that of TO and TS, to date the two most common detection parameters. Interestingly, the simulation results show that TS performs better than TO, a result that has been previously established in several clinical studies, whereas to the best of our knowledge, it is quantified for the first time with simulations. The parameter $T(\mathbf{x})$ achieves the same performance as TS with only half the number of VEBs, whereas TS achieves the same performance as TO with half the number of VEBs for averaging (Section IV-B).

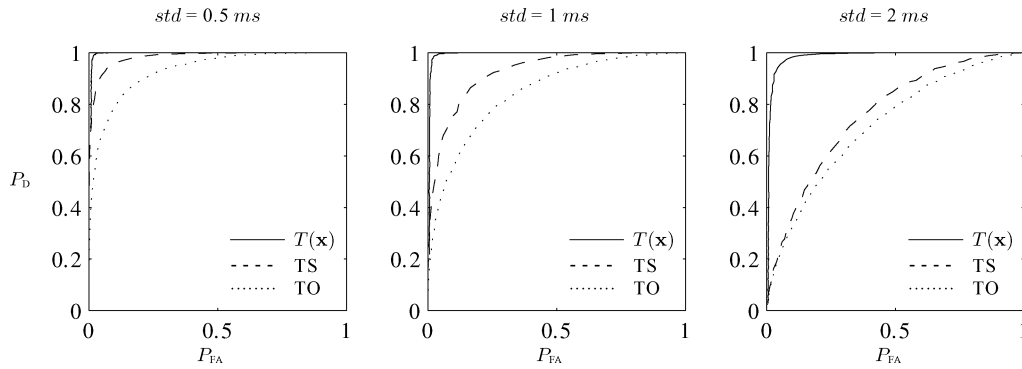


Fig. 9. ROC curves describing the influence of QRS detection inaccuracies on HRT detection, studied by QRS jitter with different standard deviations (*std*). The SNR was equal to 10 dB.

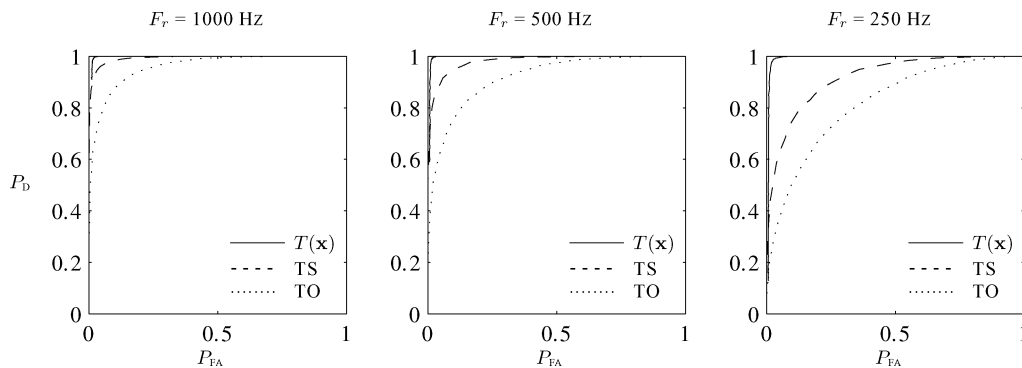


Fig. 10. ROC curves describing the influence of sampling rate F_r on HRT detection. The SNR was equal to 10 dB.

TABLE I
HRT PARAMETERS $T(\mathbf{x})$, TO, AND TS FOR THE EIGHT HiR AND HiP HEMODIALYSIS PATIENTS

Patient:	HiR					HiP				
	1	2	3	4	<i>mean</i> \pm <i>std</i>	5	6	7	8	<i>mean</i> \pm <i>std</i>
$T(\mathbf{x})$	1257	90	71	10	357 ± 601	10	3.1	2.5	0.6	4.1 ± 4.3
TO	-2.9	-0.26	1.6	0.07	-0.38 ± 1.9	-0.05	0.13	0.30	-0.06	0.08 ± 0.17
TS	3.7	1.0	1.0	1.7	1.8 ± 1.3	0.2	0.5	2.0	0.3	0.7 ± 0.9

Values are presented in descending order of $T(\mathbf{x})$.

Using a small dataset of ECGs acquired from dialysis patients, this paper shows that the model-based approach achieves better separation between patients being prone and resistant to hypotension than what is achieved with TO and TS. However, the significance of this result needs to be further established in a study where a larger dataset is used.

It would be desirable to only use subjects with HRT when computing the basis functions; however, this is not possible without having to resort to existing parameters for HRT detection. In this study, subjects with and without HRT were merged when computing the basis functions since the subjects without HRT do not contribute much to the dominant basis functions.

The GLRT statistic $T(\mathbf{x})$ in (17) was derived under the white noise assumption. While this assumption is unrealistic because the noise corresponds to spontaneous variability in heart rate, it is nonetheless adopted as no estimation of HRV spectrum is required, and accordingly, a much simpler detector structure

results. It is well known that inaccurate spectral estimates may actually cause the performance to degrade beyond that achieved by a detector based on the white noise assumption. The present HRT detector was found to have excellent performance on the simulated signals despite the fact that the detector was mismatched to the spectral HRV properties [see Fig. 3(b)].

To shed further light on the white noise assumption, it is interesting to note that TS, being employed in numerous clinical studies without much methodological discussion, can also be related to a white noise model, namely

$$x(n) = A + Bn + v(n) \quad (25)$$

where A denotes the intercept, B denotes the slope, and $v(n)$ denotes the white Gaussian noise. The MLE of B is identical to the one used to compute TS [23]. While TS is introduced from heuristic reasoning, this parameter can just as well be viewed as one associated with the statistical signal model in (25).

Undoubtedly, TS is crucial to the many HRT studies and its significance is not diminished by the underlying white noise assumption; the same observation could also apply to the present approach.

Detector performance was studied with respect to the accuracy of the QRS detector (i.e., trigger jitter) and the sampling rate of the ECG signal. The results show that the parameters TO and TS are much more sensitive to trigger jitter and lower sampling rates than is $T(\mathbf{x})$. From HRV analysis, it is well known that too low sampling rate introduces bias and uncertainty in the HF and LF/HF indices, especially when the RR interval has low variability [24], [25]. However, the significance of sampling rate in HRT analysis has previously not been reported in the literature. The present result underlines the importance of either acquiring the ECG at a high sampling rate (preferably 1000 Hz) or digitally interpolating the ECG to a high rate if the original rate is low [26]. The precision in locating the fiducial point of the QRS complex at a low sampling rate improves when interpolation is used, and accordingly, also RR interval variability. Since many HRT studies have been based on Holter recordings, where the sampling rate may be as low as 125 Hz [13], [27], [28], interpolation should be performed to optimize performance; this recommendation applies in particular to TO and TS whose performance are more sensitive to low sampling rates.

The second-order approximation to the derivative of $d_{\text{HT}}(t)$, in (7), may be interpreted as a low-pass filtered instantaneous heart rate, since the first-order approximation, $T_0/(t_k - t_{k-1} - 1)$, is a zero-mean normalized instantaneous heart rate $1/(t_k - t_{k-1})$. In the calculation of the KL basis functions and the HRT test statistic, the second-order approximation is used, since it is less sensitive to noise compared to the first-order approximation due to the low-pass filtering effect.

In the extended IPFM model, the scope of the linear system is to model the HRT shape, not the entire feedback mechanism, and therefore, the modulating signal $x(t)$ receives a feedback signal $s(t)$ triggered by the VEB. The shape of the feedback signal is modeled by the signal subspace defined by the most significant KL basis functions. A simple way to connect VEB triggering of HRT to the feedback signal is by means of a linear system whose impulse response $h_l(t)$ characterizes the turbulence feedback and whose input, composed of impulses, triggers the phenomenon. Thus, the linear system is not associated with any assumption on the interactions responsible for HRT, but it is a mathematical model of the output shape and timing of the feedback signal. While the baroreceptor response cannot be modeled as a linear system, the turbulence phenomenon, manifested as a heart rate change, may be modeled by a linear system as suggested by the 96% of the energy accounted for by the three most significant basis functions.

VI. CONCLUSION

Model-based signal processing is developed for HRT detection and characterization. The resulting technique does not only provide insight on the HRT phenomenon, but it also relates to the HRV through the IPFM model and the heart timing signal. The simulation results show that $T(\mathbf{x})$ achieves the performance

of TO and TS at a considerably lower SNR. It is also shown that $T(\mathbf{x})$ performs much better in the presence of QRS jitter and at lower ECG sampling rates than do TO and TS. The HRT test statistic $T(\mathbf{x})$ appears to be better suited for distinguishing between HtR and HtP patients, but the significance of this result needs to be further established.

APPENDIX

DERIVATION OF THE TEST STATISTIC $T(\mathbf{x})$ FROM THE GLRT IN (16)

The GLRT in (16) decides \mathcal{H}_1 if

$$L_G(\mathbf{x}) = \frac{p(\mathbf{x}; \hat{\boldsymbol{\theta}}, \hat{\sigma}_{\mathcal{H}_1}^2, \mathcal{H}_1)}{p(\mathbf{x}; \hat{\sigma}_{\mathcal{H}_0}^2, \mathcal{H}_0)} > \gamma \quad (26)$$

where

$$p(\mathbf{x}; \boldsymbol{\theta}, \sigma^2, \mathcal{H}_1) = \frac{1}{(2\pi\sigma^2)^{N/2}} \exp \left[-\frac{1}{2\sigma^2} (\mathbf{x} - \mathbf{B}\boldsymbol{\theta})^T (\mathbf{x} - \mathbf{B}\boldsymbol{\theta}) \right] \quad (27)$$

and

$$p(\mathbf{x}; \sigma^2, \mathcal{H}_0) = \frac{1}{(2\pi\sigma^2)^{N/2}} \exp \left[-\frac{1}{2\sigma^2} \mathbf{x}^T \mathbf{x} \right]. \quad (28)$$

For the linear model, $\hat{\boldsymbol{\theta}}$ is easily shown to be [23]

$$\hat{\boldsymbol{\theta}} = (\mathbf{B}^T \mathbf{B})^{-1} \mathbf{B}^T \mathbf{x} = \mathbf{B}^T \mathbf{x} \quad (29)$$

where $\mathbf{B}^T \mathbf{B} = \mathbf{I}$, since \mathbf{B} is orthogonal. The MLE of σ^2 under \mathcal{H}_1 and \mathcal{H}_0 is found by maximizing $p(\mathbf{x}; \hat{\boldsymbol{\theta}}, \sigma^2, \mathcal{H}_1)$ and $p(\mathbf{x}; \sigma^2, \mathcal{H}_0)$, respectively, over σ^2 :

$$\hat{\sigma}_{\mathcal{H}_1}^2 = \frac{1}{N} (\mathbf{x} - \mathbf{B}\hat{\boldsymbol{\theta}})^T (\mathbf{x} - \mathbf{B}\hat{\boldsymbol{\theta}}) \quad (30)$$

$$\hat{\sigma}_{\mathcal{H}_0}^2 = \frac{1}{N} \mathbf{x}^T \mathbf{x}. \quad (31)$$

Note that

$$\begin{aligned} \hat{\sigma}_{\mathcal{H}_1}^2 &= \frac{1}{N} (\mathbf{x}^T \mathbf{x} - \mathbf{x}^T \mathbf{B}\hat{\boldsymbol{\theta}} - \hat{\boldsymbol{\theta}}^T \mathbf{B}^T \mathbf{x} + \hat{\boldsymbol{\theta}}^T \mathbf{B}^T \mathbf{B}\hat{\boldsymbol{\theta}}) \\ &= \frac{1}{N} (\mathbf{x}^T \mathbf{x} - \hat{\boldsymbol{\theta}}^T \hat{\boldsymbol{\theta}}) \\ &= \hat{\sigma}_{\mathcal{H}_0}^2 - \frac{1}{N} \hat{\boldsymbol{\theta}}^T \hat{\boldsymbol{\theta}}. \end{aligned} \quad (32)$$

Hence,

$$p(\mathbf{x}; \hat{\boldsymbol{\theta}}, \hat{\sigma}_{\mathcal{H}_1}^2, \mathcal{H}_1) = \frac{1}{(2\pi\hat{\sigma}_{\mathcal{H}_1}^2)^{N/2}} \exp \left[-\frac{N}{2} \right] \quad (33)$$

and

$$p(\mathbf{x}; \hat{\sigma}_{\mathcal{H}_0}^2, \mathcal{H}_0) = \frac{1}{(2\pi\hat{\sigma}_{\mathcal{H}_0}^2)^{N/2}} \exp \left[-\frac{N}{2} \right]. \quad (34)$$

Thus, the GLRT is

$$L_G(\mathbf{x}) = \left(\frac{\hat{\sigma}_{\mathcal{H}_0}^2}{\hat{\sigma}_{\mathcal{H}_1}^2} \right)^{N/2} > \gamma. \quad (35)$$

If we let

$$T(\mathbf{x}) = \frac{N-r}{r} (L_G(\mathbf{x})^{\frac{2}{N}} - 1) > \frac{N-r}{r} (\gamma^{\frac{2}{N}} - 1) = \gamma' \quad (36)$$

which is a monotonically increasing function of $L_G(\mathbf{x})$ and therefore an equivalent test statistic, then

$$\begin{aligned} T(\mathbf{x}) &= \frac{N-r}{r} \frac{\hat{\sigma}_{\mathcal{H}_0}^2 - \hat{\sigma}_{\mathcal{H}_1}^2}{\hat{\sigma}_{\mathcal{H}_1}^2} \\ &= \frac{N-r}{r} \frac{\hat{\boldsymbol{\theta}}^T \hat{\boldsymbol{\theta}}}{\mathbf{x}^T \mathbf{x} - \hat{\boldsymbol{\theta}}^T \hat{\boldsymbol{\theta}}} > \gamma'. \end{aligned} \quad (37)$$

REFERENCES

- [1] G. Schmidt, M. Malik, P. Barthel, R. Schneider, K. Ulm, L. Rolnitzky, A. J. Camm, J. T. Bigger, and A. Schömig, "Heart-rate turbulence after ventricular premature beats as a predictor of mortality after acute myocardial infarction," *Lancet*, vol. 353, pp. 1390–1396, 1999.
- [2] R. Schneider, P. Barthel, and M. Watanabe, "Heart rate turbulence on Holter," in *Dynamic Electrocardiography*, M. Malik and A. J. Camm, Eds. New York: Futura, 2004, ch. 20, pp. 190–193.
- [3] M. Watanabe and G. Schmidt, "Heart rate turbulence: A 5-year review," *Heart Rhythm*, vol. 1, pp. 732–738, 2004.
- [4] M. Watanabe, "Heart rate turbulence: A review," *Indian Pacing Electro-physiol. J.*, vol. 3, pp. 10–22, 2003.
- [5] S. Raj, R. Sheldon, M. Koshman, and D. Roach, "Role of hypotension in turbulence physiology," *Heart Rhythm*, vol. 2, pp. 710–717, 2005.
- [6] M. Watanabe, "Role of hypotension in heart rate turbulence," *Heart Rhythm*, vol. 2, pp. 828–829, 2005.
- [7] A. Bauer and G. Schmidt, "Last piece of the heart rate turbulence puzzle?" *Heart Rhythm*, vol. 4, pp. 290–291, 2007.
- [8] K. Solem, A. Nilsson, and L. Sörnmo, "An electrocardiogram-based method for early detection of abrupt changes in blood pressure during hemodialysis," *ASAIO J.*, vol. 52, pp. 282–290, 2006.
- [9] A. Hallstrom, P. Stein, R. Schneider, M. Hodges, G. Schmidt, and K. Ulm, "Structural relationships between measures based on heart beat intervals: Potential for improved risk assessment," *IEEE Trans. Biomed. Eng.*, vol. 51, no. 8, pp. 1414–1420, Aug. 2004.
- [10] M. Watanabe, J. Marine, R. Sheldon, and M. Josephson, "Effects of ventricular premature stimulus coupling interval on blood pressure and heart rate turbulence," *Circulation*, vol. 106, pp. 325–330, 2002.
- [11] G. Schmidt, R. Schneider, and P. Barthel, "Correlation coefficient of the heart rate turbulence slope: New risk stratifier in post-infarction patients," *Eur. Heart J.*, vol. 22, p. 72, 2001 (P484).
- [12] A. Berkowitsch, N. Guettler, T. Neumann, D. Vukajlovic, B. Schulte, J. Neuzner, and H. Pitschner, "Turbulence jump—A new descriptor of heart-rate turbulence after paced premature ventricular beats. A study in dilated cardiomyopathy patients," *Eur. Heart J.*, vol. 22, p. 547, 2001 (P2941).
- [13] A. Bauer, M. Malik, P. Barthel, R. Schneider, M. Watanabe, A. Camm, A. Schömig, and G. Schmidt, "Turbulence dynamics: An independent predictor of late mortality after acute myocardial infarction," *Int. J. Cardiol.*, vol. 107, pp. 42–47, 2006.
- [14] B. W. Hyndman and R. K. Mohn, "A model of the cardiac pacemaker and its use in decoding the information content of cardiac intervals," *Automedica*, vol. 1, pp. 239–252, 1975.
- [15] L. Sörnmo and P. Laguna, *Bioelectrical Signal Processing in Cardiac and Neurological Applications*. Amsterdam, The Netherlands: Elsevier, 2005.
- [16] J. Mateo and P. Laguna, "Improved heart rate variability signal analysis from the beat occurrence times according to the IPFM model," *IEEE Trans. Biomed. Eng.*, vol. 47, no. 8, pp. 997–1009, Aug. 2000.
- [17] A. J. Vander, J. H. Sherman, and D. S. Luciano, *Human Physiology*. New York: McGraw-Hill, 1990.
- [18] S. M. Kay, *Fundamentals of Statistical Signal Processing, Vol. II: Detection Theory*. Upper Saddle River, NJ: Prentice-Hall, 1998.
- [19] P. Laguna, G. B. Moody, and R. G. Mark, "Power spectral density of unevenly sampled data by least-square analysis: Performance and application to heart rate signals," *IEEE Trans. Biomed. Eng.*, vol. 45, no. 6, pp. 698–715, Jun. 1998.
- [20] A. Taddei, G. Distante, M. Emdin, P. Pisani, G. B. Moody, C. Zeelenberg, and C. Marchesi, "The European ST-T database: Standards for evaluating systems for the analysis of ST-T changes in ambulatory electrocardiography," *Eur. Heart J.*, vol. 13, pp. 1164–1172, 1992.
- [21] J. Mateo and P. Laguna, "Analysis of heart rate variability in the presence of ectopic beats using the heart timing signal," *IEEE Trans. Biomed. Eng.*, vol. 50, no. 3, pp. 334–343, Mar. 2003.
- [22] K. Solem, P. Laguna, and L. Sörnmo, "An efficient method for handling ectopic beats using the heart timing signal," *IEEE Trans. Biomed. Eng.*, vol. 53, no. 1, pp. 13–20, Jan. 2006.
- [23] S. M. Kay, *Fundamentals of Statistical Signal Processing, Vol. I: Estimation Theory*. Upper Saddle River, NJ: Prentice-Hall, 1993.
- [24] M. Merri, D. C. Farden, J. G. Mottley, and E. L. Titlebaum, "Sampling frequency of the electrocardiogram for spectral analysis of the heart rate variability," *IEEE Trans. Biomed. Eng.*, vol. 37, no. 1, pp. 99–106, Jan. 1990.
- [25] M. A. García-González, M. Fernández-Chimeno, and J. Ramos-Castro, "Bias and uncertainty in heart rate variability spectral indices due to the finite ECG sampling frequency," *Physiol. Meas.*, vol. 25, pp. 489–504, 2004.
- [26] P. Laguna and L. Sörnmo, "Sampling rate and the estimation of ensemble variability for repetitive signals," *Med. Biol. Eng. Comput.*, vol. 38, pp. 540–546, 2000.
- [27] A. Iwasa, M. Hwa, A. Hassankhani, T. Liu, and S. Narayan, "Abnormal heart rate turbulence predicts the initiation of ventricular arrhythmias," *Pace*, vol. 28, pp. 1189–1197, 2005.
- [28] A. Bauer, M. Watanabe, P. Barthel, R. Schneider, K. Ulm, and G. Schmidt, "QRS duration and late mortality in unselected post-infarction patients of the revascularization era," *Eur. Heart J.*, vol. 27, pp. 427–433, 2006.



Kristian Solem received the M.Sc. degree in electrical engineering in 2003 from Lund University, Lund, Sweden, where he is currently working toward the Ph.D. degree in signal processing and its application to biomedical signals.

His current research interests include ECG signals and their significance in heart rate variability analysis, heart rate turbulence analysis, and hemodialysis. He is also involved in teaching courses in signal processing.



Pablo Laguna (M'92–SM'06) was born in Jaca, Spain, in 1962. He received the M.S. degree in physics and the Ph.D. degree in physics from the Science Faculty, University of Zaragoza, Zaragoza, Spain, in 1985 and 1990, respectively.

He is currently a Full Professor of signal processing and communications in the Department of Electrical Engineering, Engineering School, University of Zaragoza, where he is also a Researcher at the Aragón Institute for Engineering Research (I3A), where from 1992 to 2005, he was an Associate Professor. From 1987 to 1992, he was an Assistant Professor of automatic control in the Department of Control Engineering, Politecnico University of Catalonia (U.P.C.), Spain, and as a Researcher at the Biomedical Engineering Division, Institute of Cybernetics (U.P.C.–C.S.I.C.). He is also with the Networking Biomedical Research Centro de Investigación Biomédica en Red en Bioingeniería, Biomateriales y Nanomedicina (CIBER-BBN), Zaragoza. His current research interests include signal processing, in particular applied to biomedical applications. He is the author of the book *Bioelectrical Signal Processing in Cardiac and Neurological Applications* (Elsevier, 2005).



Juan Pablo Martínez was born in Zaragoza, Spain, in 1976. He received the M.S. degree in telecommunication engineering and the Ph.D. degree in biomedical engineering from the University of Zaragoza (UZ), Zaragoza, in 1999 and 2005, respectively.

Since 2000, he has been an Assistant Professor in the Department of Electronic Engineering and Communications, UZ, where since 2007, he has been an Associate Professor, and is also a Researcher at the Aragón Institute for Engineering Research (I3A). He is also with the Centro de Investigación Biomédica en Red en Bioingeniería, Biomateriales y Nanomedicina (CIBER-BBN), Zaragoza. His current research interests include biomedical signal processing, with main interest in signals of cardiovascular origin.



Leif Sörnmo (S'77–M'84–SM'02) received the M.Sc. and Ph.D. degrees in electrical engineering from Lund University, Lund, Sweden, in 1978 and 1984, respectively.

From 1983 to 1995, he was engaged in problems in computer-based ECG analysis in the Department of Clinical Physiology, Lund University, where since 1990, he has been with the Signal Processing Group, Department of Electrical and Information Technology, and is currently a Professor in biomedical signal processing. His current research interests include statistical signal processing and modeling of biomedical signals, methods for atrial fibrillation analysis, multimodal signal processing in hemodialysis, detection of otoacoustic emissions, and power efficient signal processing in implantable devices. He is the author of the book *Bioelectrical Signal Processing in Cardiac and Neurological Applications* (Elsevier, 2005). He has been an Associate Editor of the *Computers in Biomedical Research* (1997–2000). He is currently an Associate Editor of the *Journal of Electrocardiology*, and on the Editorial Board of the *Medical and Biological Engineering and Computing*.

Dr. Sörnmo is currently an Associate Editor of the IEEE TRANSACTIONS ON BIOMEDICAL ENGINEERING.